Geophysical Research Letters

Supporting Information for

Towards narrowing uncertainty in future projections of local extreme precipitation

Francesco Marra[1,2,*], Moshe Armon[1], Ori Adam[1], Davide Zoccatelli[1], Osama Gazal[3], Chaim I. Garfinkel[1], Dorita Rostkier-Edelstein[1,4], Uri Dayan[5], Yehouda Enzel[1], and Efrat Morin[1]

[1]The Fredy and Nadine Herrmann Institute of Earth Sciences, The Hebrew University of Jerusalem, Israel

[2]Institute of Atmospheric Sciences and Climate, National Research Council of Italy, CNR-ISAC, Bologna, Italy

[3]Faculty of Agricultural and Environmental Sciences, Szent Istvan University, Hungary

[4]Department of Environmental Physics, Environmental Sciences Division, IIBR, Ness-Ziona, Israel

[5]Department of Geography, The Hebrew University of Jerusalem, Israel

Contents of this file

Code	Alpert et al. (2004)	Precipitation type in this study
1	Red Sea Trough with the Eastern axis	2
2	Red Sea Trough with the Western axis	2
3	Red Sea Trough with the Central axis	2
4	Persian Trough (Weak)	3
5	Persian Trough (Medium)	3
6	Persian Trough (Deep)	3
7	High to the East	3
8	High to the West	3
9	High to the North	3
10	High over Israel (Central)	3
11	Low to the East (Deep)	1
12	Cyprus Low to the South (Deep)	1
13	Cyprus Low to the South (Shallow)	1
14	Cyprus Low to the North (Deep)	1
15	Cyprus Low to the North (Shallow)	1
16	cold Low to the West	1
17	Low to the East (Shallow)	1
18	Sharav Low to the West	2
19	Sharav Low over Israel (Central)	2

Table S1. Synoptic systems in the semi-automatic classification by Alpert at al. (2004) and corresponding precipitation types used in this study, as follows: (1) *Type-1* (Mediterranean cyclones), (2) *Type-2* (other type of systems), (3) individually examined and labelled as *Type-1* if occurring up to 2 days after a *Type-1* wet day, and as *Type-2* in the remaining cases

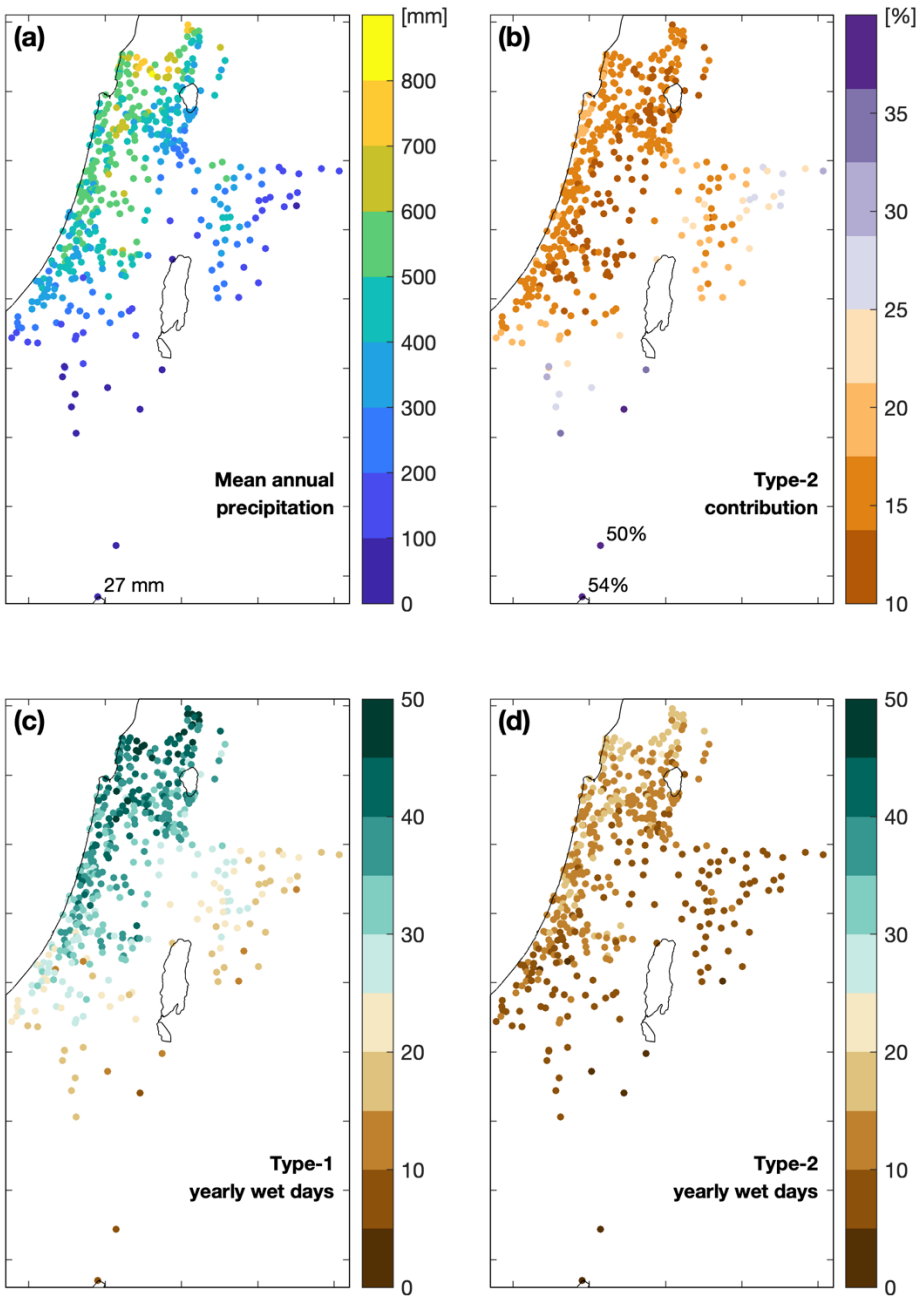

Figure S1. Mean annual precipitation. (a) Mean annual precipitation in the south-eastern Mediterranean. Precipitation is mainly contributed by Mediterranean cyclones (*Type-1*) as shown in the other panels. (b) Relative contribution to the mean annual precipitation from *Type-2* events. Average yearly number of *Type-1* (c) and *Type-2* (d) wet days.

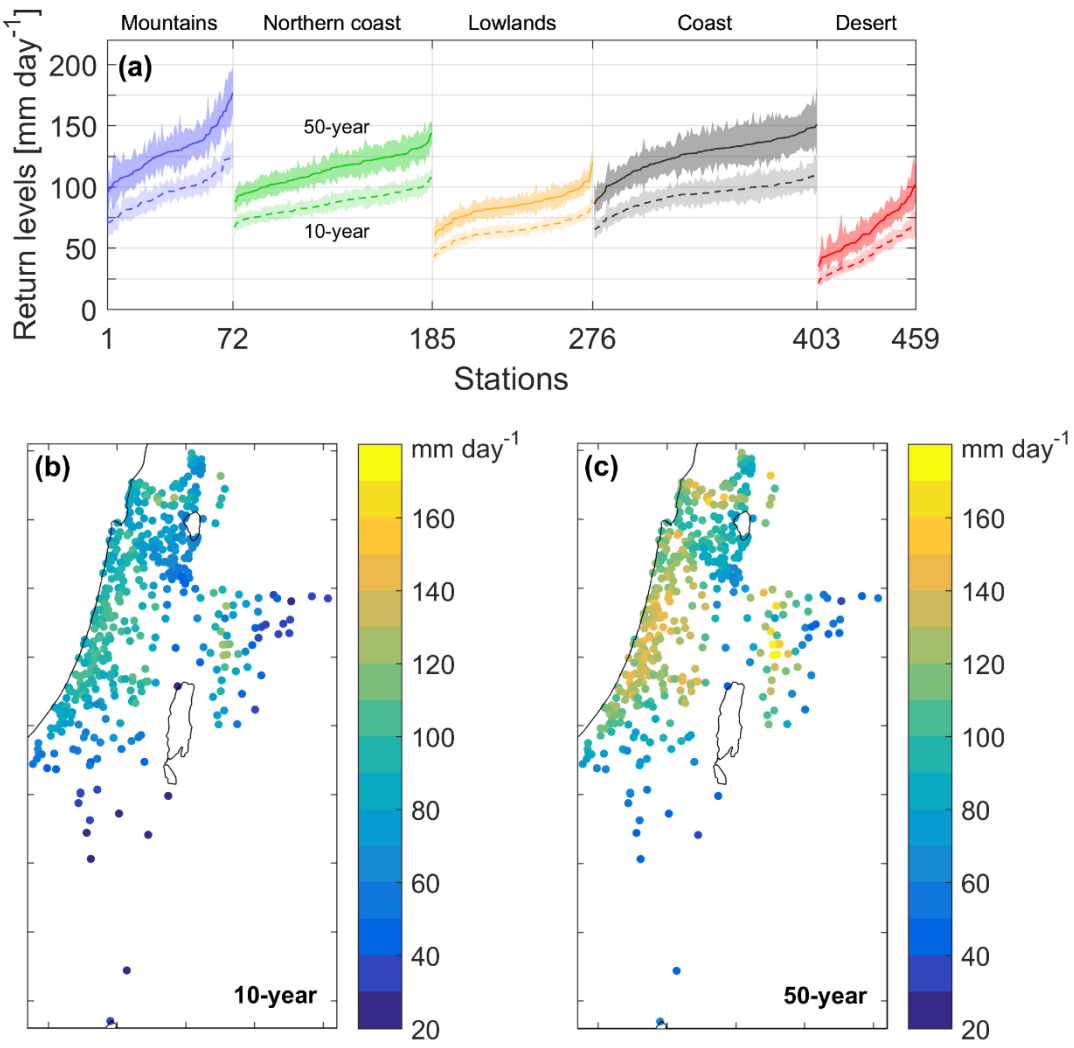

Figure S2. (a) Distribution of return levels and relative uncertainty (90% confidence interval from 103 bootstrap samples with replacement among the years in the record) shown as transposed cumulative distributions; colors refer to for the five groups of stations in Fig. 1a. (b, c) Map of the 10-year (c) and 50-year (d) return levels (10% and 2% yearly exceedance probability).

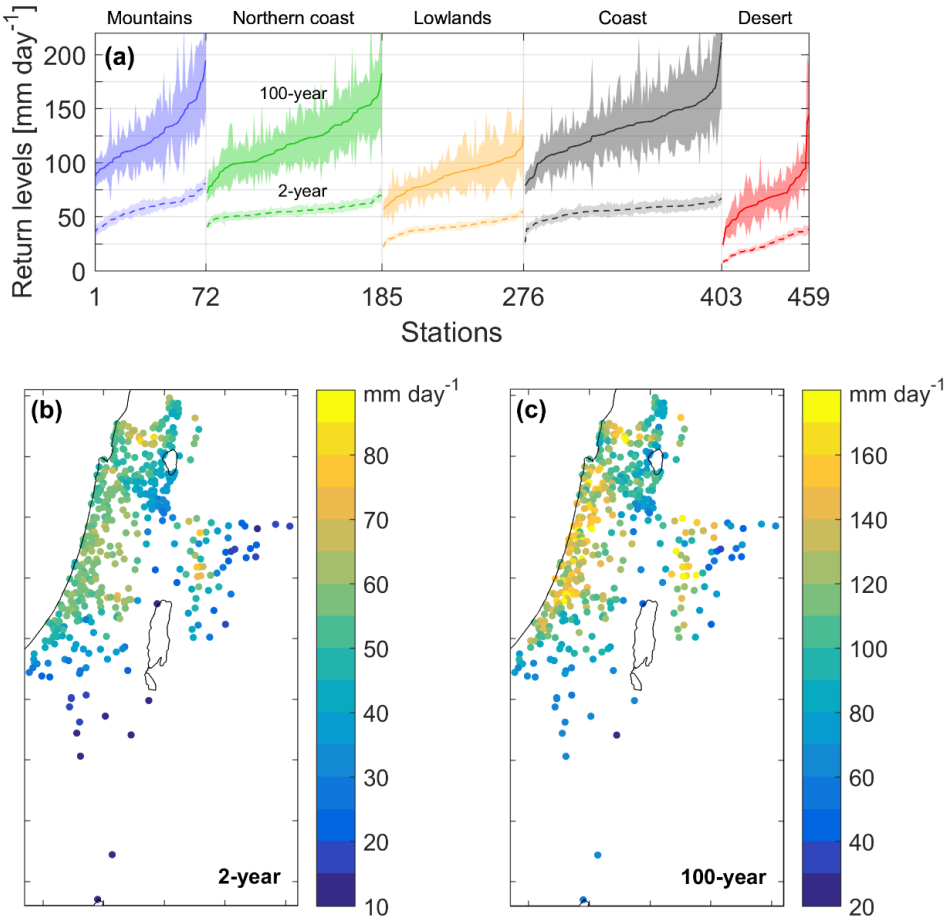

Figure S3. Extreme return levels computed using traditional approaches. Two-year and 100-year return levels (50% and 1% yearly exceedance probability) for daily precipitation amounts computed using traditional methods based on extreme value theory: a Generalized Extreme Value distribution is fitted to the annual maxima series using the method of the L-moments (Hosking, 1990). (a) Distribution of return levels and relative uncertainty (90% confidence interval from 103 bootstrap samples with replacement among the years in the record) shown as transposed cumulative distributions; median uncertainty of 17% (39%) for 2-year (100-year) return levels. The colors of the five groups of stations are as in Fig. 1a. (b, c) Map of the 2-year (c) and 100-year (d) return levels (50% and 1% yearly exceedance probability). Note the larger spatial variability (noise) of the return levels relative to Fig. 1, reflecting the largely increased uncertainty characterizing traditional methods based on the analysis of observed extremes (here, the annual maxima).

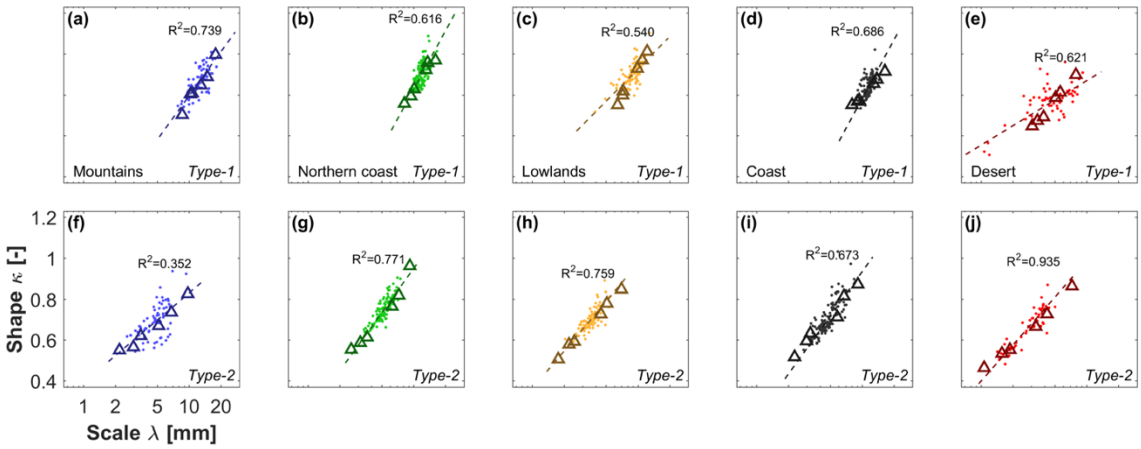

Figure S4. Local constraints of the parameters of the intensity distribution of the ordinary events. Scatter plot of the scale (λ) and shape (κ) parameters of the observed Weibull distributions for the two types of ordinary events and for the five groups of stations; colors as in Fig. 1a. The regressions used to define the local constraints (α coefficients) are shown as dashed lines. Triangles represent the median (among stations) parameters obtained using, for each station, groups of five non-consecutive years with increasing median intensity of the ordinary events.

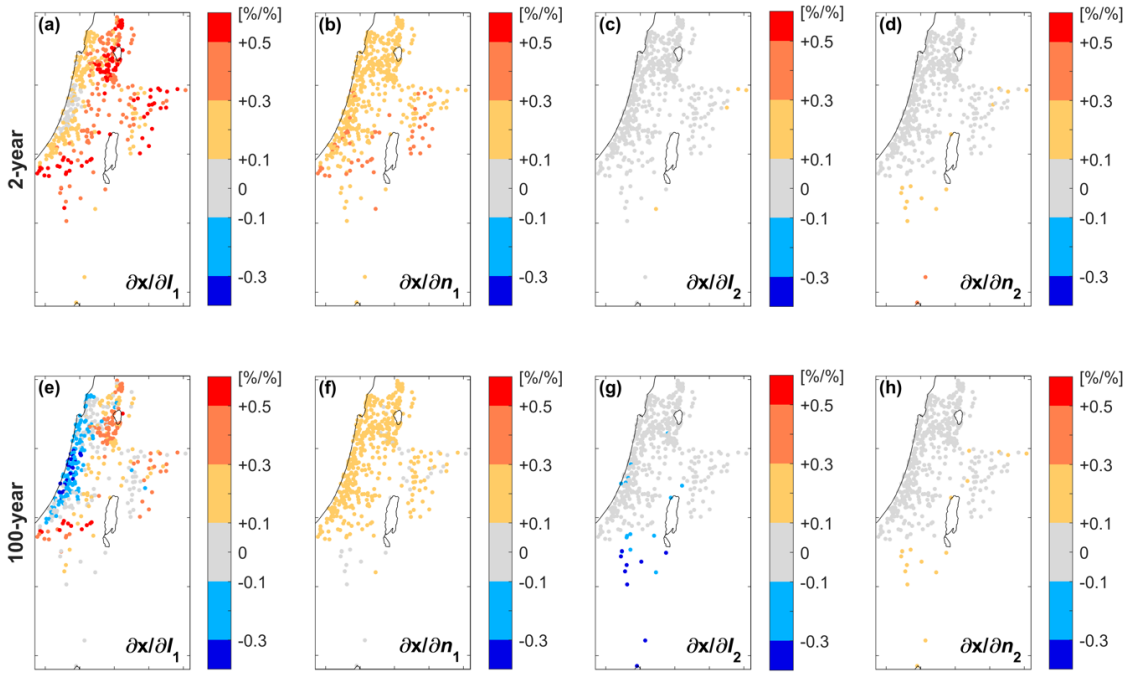

Figure S5. Sensitivity of extreme return levels to changes in the average characteristics of ordinary events. Sensitivity of 2-year (a-d) and 100-year (e-h) return levels (50% and 1% yearly exceedance probability) to changes in median intensity (I) and expected number of yearly occurrence (n) of the two types of ordinary events. The sensitivity or extreme return levels $x(p)$ to changes in the median intensity and in the expected number of ordinary events is computed numerically using the partial derivatives of $x(p) = \zeta^{(-1)}(p; I_1, n_1; I_2, n_2)$ with respect to the four variables, i.e., $\frac{\partial x(p)}{\partial I_1}$, $\frac{\partial x(p)}{\partial I_2}$, $\frac{\partial x(p)}{\partial n_1}$, and $\frac{\partial x(p)}{\partial n_2}$. Units of change in x per 1% change in the predictor are quantified. The figure highlights two important points. First, different return levels can have different responses. Since practical applications rely on different return levels, this implies that the potential impact of climate change strongly depends on the application of interest. For instance, sewer systems are generally designed to be overtopped not more than once in 2-5 years. In contrast, dams, bridges and river dikes are designed for much lower probabilities of failure (e.g., 100- or even 1000-year). Second, the local sensitivities associated with each type of event can differ significantly. Therefore, local changes in extremes are related to mean (or median) changes in precipitation in a complex manner.

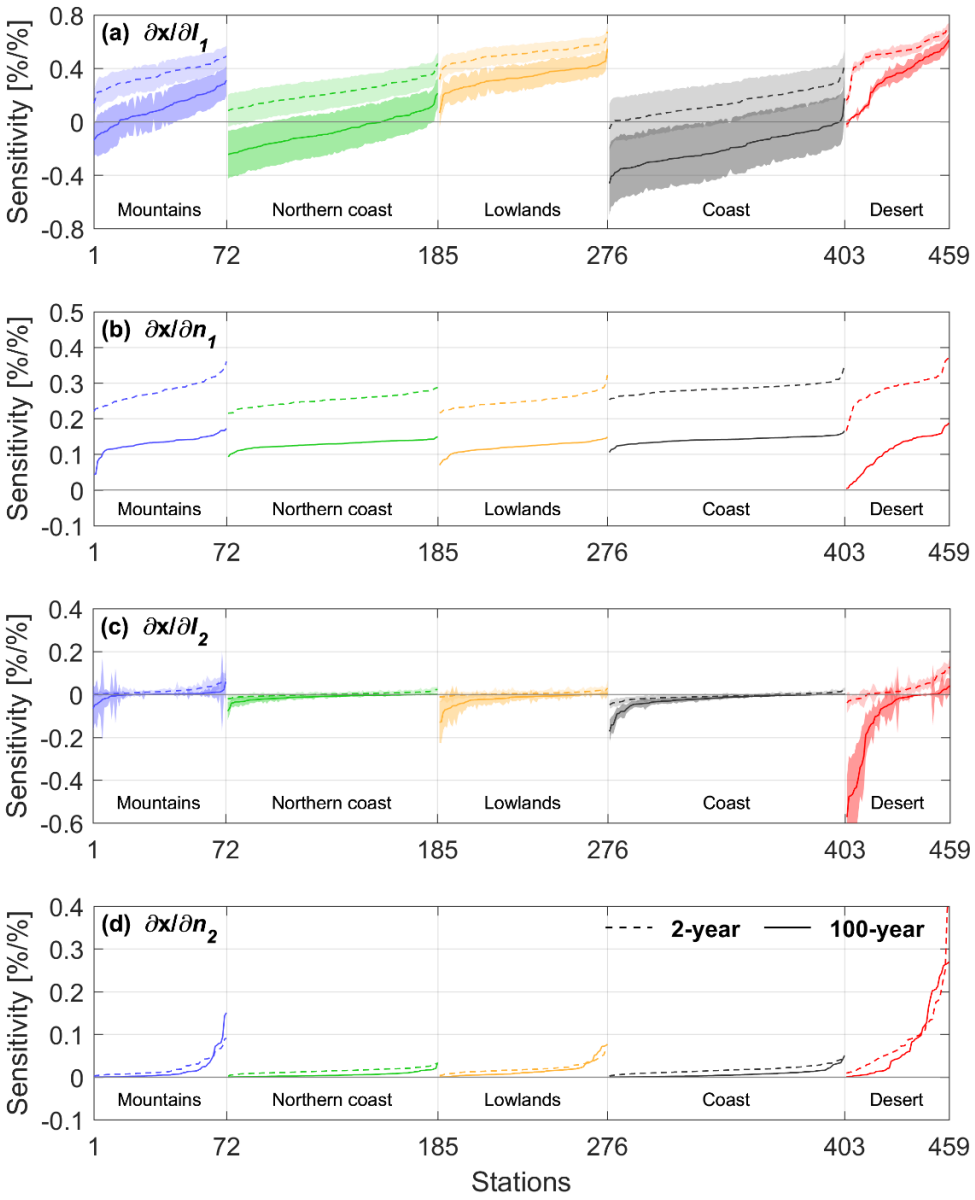

Figure S6. Sensitivity of extreme return levels to changes in the ordinary events. Distribution of the sensitivity of 2-year and 100-year return levels to changes in the average characteristics of the two types ordinary events shown as transposed cumulative distributions; uncertainties in the sensitivity to the median intensities are computed as 90% confidence interval of the local constrains (90% confidence interval of the α coefficients). (a) Sensitivity to the *Type-1* intensity. (b) Sensitivity to the *Type-1* yearly number of events. (c) Sensitivity to the *Type-2* intensity. (d) Sensitivity to the *Type-2* yearly number of events.

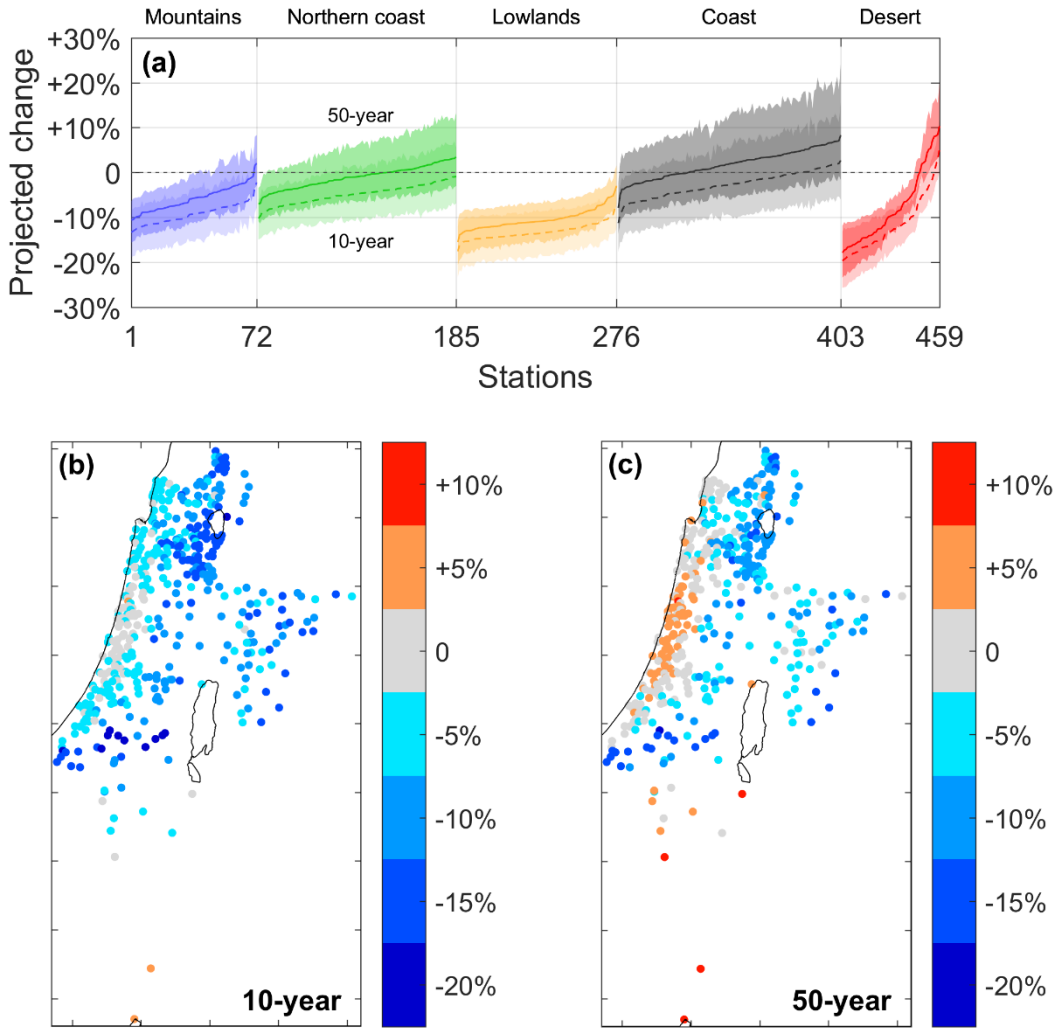

Figure S7. Projected changes in extreme precipitation return levels (RCP8.5 emission scenario; 10-year and 50-year return levels). Projected changes in 10-year and 50-year return levels (10% and 2% yearly exceedance probability) for the end of the century (difference between ~2080-2100 and ~1980-2005) under the RCP8.5 emission scenario. (a) Distribution of the projected change and relative uncertainty (90% confidence interval considering uncertainties in climate projections and local constraints) shown as transposed cumulative distributions; colors as in Fig. 1a. (b-c) Map of the projected change for the 10-year (b) and 50-year (c) return levels.

References

Alpert P, Osetinsky I, Ziv B, Shafir H 2004 Semi-Objective Classification for Daily Synoptic Systems: Application to the Eastern Mediterranean Climate Change. Int. J. Climatol. 24(8), 1001–11

Hosking JRM 1990 L-moments: Analysis and estimation of distributions using linear combinations of order statistics. J. Royal Stat. Soc. B, 52(1), 105–124